The Science of Making Torque from Wind IOP Publishing
Journal of Physics: Conference Series **75** (2007) 012079 doi:10.1088/1742-6596/75/1/012079

# Performance comparison of control schemes for variable-speed wind turbines

**C L Bottasso, A Croce, B Savini**

Dipartimento di Ingegneria Aerospaziale, Politecnico di Milano, Via La Masa 34
I-20156 Milano, Italy

E-mail: carlo.bottasso@polimi.it

**Abstract.**

We analyze the performance of different control schemes when applied to the regulation problem of a variable-speed representative wind turbine. In particular, we formulate and compare a wind-scheduled PID, a LQR controller and a novel adaptive non-linear model predictive controller, equipped with observers of the tower states and wind. The simulations include gusts and turbulent winds of varying intensity in nominal as well as off-design operating conditions. The experiments highlight the possible advantages of model-based non-linear control strategies.

## 1. Wind turbine models

This paper presents some intermediate results of an ongoing research activity on the active control of variable-speed wind turbines. In this paper we consider the torque and collective pitch control problem, and we evaluate the performance of different control schemes in a simulated environment. These are intermediate steps towards more ambitious long-term goals of the project, which also call for the testing in the field of model-based individual-blade controllers.

In this paper we use two different models of a representative 1.5MW wind turbine. The first one is an high-fidelity fine-scale aeroelastic model based on a multibody approach, which is used for simulating the plant. The second one is a reduced coarse-scale model used by the model-based controllers; scope of this model is to capture of the to-be-controlled response of the plant with only relatively few degrees of freedom.

### *1.1. Aeroelastic wind turbine model*

In this work, we use a finite-element-based multibody formulation that is more thoroughly described in Ref. [2]. The multibody formulation is based on the full finite-element method, which means that no modal-based reduction is performed on the deformable components of the structure. Cartesian coordinates are used for the description of all entities in the model, and all degrees of freedom are referred to a single inertial frame; the formulation handles arbitrarily large three-dimensional rotations.

The turbine blades and tower are modeled by beam elements. The element models beams of arbitrary geometry, including curved and twisted reference lines, and accounts for axial, shear, bending, and torsional stiffness. Joints are modeled through holonomic or nonholonomic constraints, as appropriate, which are enforced by means of Lagrange multipliers using the

augmented Lagrangian method. All joints can be equipped with internal springs, dampers, backlash, and friction models.

Lifting lines can be associated with beam elements and are described by three-dimensional twisted curves, which do not necessarily coincide with the associated beam reference lines. The lifting lines are based on classical two-dimensional blade element theory and use local profile aerodynamic characteristics, accounting for the aerodynamic center offset, twist, sweep, and unsteady corrections. Lifting lines are used here to model the aerodynamic characteristics of the blades, but also of the tower and of the nacelle. An inflow element can be associated with the blade lifting lines to model the rotor inflow effects; presently, the Peters-He and the dynamic Pitt-Peters wake models [5] are implemented in the code. Tip and hub loss models are also considered.

Wind is modeled as the sum of a steady state mean wind and a perturbation wind, accounting for turbulence and/or gusts. The deterministic component of the wind field implements the transients specified by IEC 61400-1 [1], the exponential and logarithmic wind shear models, and the tower shadow effects, which include the potential flow model for a conical tower, the downwind empirical model based on Ref. [6], or an interpolation of these two models. The stochastic component of the wind field is computed according to the Von Karman or Kaimal turbulence models. The turbulent wind is precomputed before the beginning of the simulation for an assigned duration of time and for a user-specified two-dimensional grid of points. During the simulation, the current position of each airstation is mapped to this grid, and the current value of the wind is interpolated in space and time from the saved data.

The multibody formulation used in this effort leads to a set of nonlinear partial differential algebraic equations. Spatial discretization of the flexible components using the finite-element method yields a system of differential algebraic equations in time, which are solved using an implicit integration procedure that is nonlinearly unconditionally stable. The implicit nature of the scheme allows for the use of large time steps and is more appropriate than explicit schemes for the typical dynamics of rotor systems. At each time step, the resulting nonlinear system of equations is solved using a quasi-Newton scheme. The time-step length is adjusted based on an error indicator.

*1.2. Reduced wind turbine model*

The non-linear reduced model of the turbine used by the model-based controllers includes drive-train shaft dynamics, elastic tower fore-aft motion, blade pitch actuator dynamics and electrical generator dynamics:

$$(J_R + J_G)\dot{\Omega} + T_l(\Omega) + T_{el_e} - T_a(\Omega, \beta_e, V_w - \dot{d}, V_m) = 0, \quad (1)$$

$$M_T\ddot{d} + C_T\dot{d} + K_T d - F_a(\Omega, \beta_e, V_w - \dot{d}, V_m) = 0, \quad (2)$$

$$\ddot{\beta}_e + 2\xi\omega\dot{\beta}_e + \omega^2(\beta_e - \beta_c) = 0, \quad (3)$$

$$\dot{T}_{el_e} + \frac{1}{\tau}(T_{el_e} - T_{el_c}) = 0. \quad (4)$$

The first equation, Eq. (1), describes the drive-train dynamics; $\Omega$ is the rotor angular velocity, $d$ is the tower top fore-aft displacement and $\beta_e$ is the effective blade pitch angle. Moreover, $J_R$ is the sum of the moments of inertia about the rotation axis of the rotor hub and of the three rotor blades, while $J_G$ is the moment of inertia of the rotating part of the electric generator. The torques acting upon the drive-train include the mechanical losses on the shaft bearings $T_l$, the effective electrical reaction torque $T_{el_e}$ and the aerodynamic torque $T_a$. The mechanical loss $T_l$ is modeled by means of a speed-torque look-up table. Deformations of the rotor drive-train are not included in the model, since the generator is directly driven in the machine modeled here. The second equation, Eq. (2), models the fore-aft tower dynamics. Here, $M_T$, $C_T$ and $K_T$

are, respectively, the tower equivalent modal mass, structural damping and bending stiffness. These quantities were obtained by modal reduction of a detailed finite element model of the tower. Finally, $F_a$ indicates the aerodynamic force produced by the rotor. The third equation, Eq. (3), is a second order model of the blade pitch actuator, where $\omega$ is the undamped natural frequency, $\xi$ the damping factor, and $\beta_c$ the blade pitch control. The model also includes upper and lower limits on the pitch and the pitch rate. The fourth and last equation, Eq. (4), is a first order model of the electrical generator that includes a time delay $\tau$, while $T_{el_c}$ is the commanded electrical torque input.

The rotor aerodynamic force and torque are computed as

$$T_a = \frac{1}{2}\rho\pi R^3 \frac{C_{P_e}(\lambda, \beta_e, V_m)}{\lambda}(V_w - \dot{d})^2, \tag{5}$$

$$F_a = \frac{1}{2}\rho\pi R^2 C_{F_e}(\lambda, \beta_e, V_m)(V_w - \dot{d})^2, \tag{6}$$

where $\rho$ is the air density, $C_{P_e}$ and $C_{F_e}$ the effective power and force coefficients, respectively, and $\lambda$ is the tip-speed ratio, defined as $\lambda = \Omega R/(V_w - \dot{d})$. Finally, $V_w = V_m + V_t$ is the turbulent upstream wind speed obtained as the sum of the mean wind $V_m$ and the turbulent wind $V_t$.

All wind velocity time histories used in the present work were computed in agreement with the IEC-61400-1 [1] standard requirements for a Category A Class I wind turbine generator. For the reduced model, the mean wind $V_m$ is computed by spatially averaging over the rotor disk the wind speed profile given by the power law [1]. Similarly, the longitudinal turbulent wind $V_m$ is defined, at each time step, as the spatial average over the rotor disk of the Kaimal turbulence model centered at the hub.

The aerodynamic coefficients $C_{P_e}$ and $C_{F_e}$ are computed off-line using the fine-scale aeroelastic model. Several simulations were run, each one for given constant values of blade pitch, mean wind speed and electric torque, until the solution settled on a periodic orbit. In these simulations the wind blowing on the rotor includes the wind shear effect, while the turbulent wind component is turned off. The power and force coefficients are then computed by averaging the periodic responses over a rotor revolution; similarly, the averaged tip-speed ratio is computed. Finally, the power and force coefficients are stored in a look-up table to be used by the reduced model, the entries of the table being $\lambda$, the blade pitch $\beta_e$ and the mean wind speed $V_m$.

The dependence of the power and force coefficients in Eqs. (5) and (6) on the wind speed $V_m$, typically neglected, accounts for the deformability of tower and blades under high winds; it was seen that, for the 1.5MW turbine used in the present study, the inclusion of this effect is not negligible. For example, the maximum of the $C_{P_e}$ curve computed for 1 m/sec and for 10 m/sec changes of about 9%.

## 2. Turbine state observer

The reduced model of Eqs. (1–4) includes the tower top displacement and velocity, which are here reconstructed from the readings of accelerometers and strain gages using a Kalman Filter (KF) [7].

We consider a modal description of the tower fore-aft displacement, written as

$$d(s,t) = \sum_{j=1}^{N_m} \Phi_j(s) q_j(t), \tag{7}$$

where $d(s,t)$ is the displacement at the location $s$ along the tower and at time $t$, while $\Phi_j(s)$ is the j-th modal shape, $q_j(t)$ its associated modal amplitude and $N_m$ the number of modes.

The accelerations at the locations $\boldsymbol{s}_a = (s_{a_1}, s_{a_2}, \ldots, s_{a_{N_a}})^T$ along the tower can be obtained by taking the second derivative with respect to time of Eq. (7), which yields

$$\ddot{\boldsymbol{d}} = \boldsymbol{\Phi}\ddot{\boldsymbol{q}}, \tag{8}$$

where the vector of tower displacements is defined as $\boldsymbol{d} = (d(s_{a_1}, t), d(s_{a_2}, t), \ldots, d(s_{a_{N_a}}, t))^T$, $\boldsymbol{\Phi} = [\Phi_{ij}] = [\Phi_j(s_{a_i})]$ is a matrix of tower modal shapes evaluated at the $\boldsymbol{s}_a$ locations, and $\boldsymbol{q} = (q_1(t), q_2(t), \ldots, q_{N_m}(t))^T$ is a vector of modal amplitudes. Accelerometers located at $\boldsymbol{s}_a$ provide readings $\boldsymbol{a}$ of the tower accelerations affected by a white noise $\boldsymbol{n}_w$, i.e.

$$\ddot{\boldsymbol{d}} = \boldsymbol{a} + \boldsymbol{n}_w. \tag{9}$$

Therefore, the tower fore-aft dynamics can be expressed by the following state equations in first order form:

$$\left\{ \begin{array}{lcl} \dot{\boldsymbol{q}} & = & \boldsymbol{v}, \\ \dot{\boldsymbol{v}} & = & \boldsymbol{\Psi}(\boldsymbol{a} + \boldsymbol{n}_w), \end{array} \right. \tag{10}$$

where $\boldsymbol{\Psi} = (\boldsymbol{\Phi}^T\boldsymbol{\Phi})^{-1}\boldsymbol{\Phi}^T$ and $N_a \geq N_m$, $\boldsymbol{v}$ being modal velocities.

The curvatures at the locations $\boldsymbol{s}_s = (s_{s_1}, s_{s_2}, \ldots, s_{s_{N_s}})^T$ along the tower can be obtained by taking the second derivative with respect to $s$ of Eq. (7), which yields

$$\boldsymbol{d}'' = \boldsymbol{\Phi}''\boldsymbol{q}, \tag{11}$$

where $\boldsymbol{\Phi}'' = [\Phi''_{ij}] = [\Phi''_j(s_{s_i})]$ is a matrix of tower modal curvatures. Strain gages located at $\boldsymbol{s}_s$ provide readings $\boldsymbol{c}$ of the tower curvatures affected by a white noise $\boldsymbol{n}_v$, i.e.

$$\boldsymbol{d}'' = \boldsymbol{c} + \boldsymbol{n}_v. \tag{12}$$

This defines a set of measured outputs $\boldsymbol{c}$ related to the state variables $\boldsymbol{q}$ as

$$\boldsymbol{c} = \boldsymbol{\Phi}''\boldsymbol{q} - \boldsymbol{n}_v. \tag{13}$$

Equations (10) and (13) can be written in the usual state-space form as

$$\left\{ \begin{array}{lcl} \dot{\boldsymbol{x}} & = & \boldsymbol{A}\boldsymbol{x} + \boldsymbol{B}\boldsymbol{u} + \boldsymbol{W}\boldsymbol{n}_w, \\ \boldsymbol{y} & = & \boldsymbol{C}\boldsymbol{x} + \boldsymbol{D}\boldsymbol{u} + \boldsymbol{V}\boldsymbol{n}_v, \end{array} \right. \tag{14}$$

by defining $\boldsymbol{x} = (\boldsymbol{q}^T, \boldsymbol{v}^T)^T$, $\boldsymbol{u} = \boldsymbol{a}$, $\boldsymbol{y} = \boldsymbol{c}$ and

$$\boldsymbol{A} = \left[ \begin{array}{cc} \boldsymbol{0} & \boldsymbol{I} \\ \boldsymbol{0} & \boldsymbol{0} \end{array} \right], \boldsymbol{B} = \left[ \begin{array}{c} \boldsymbol{0} \\ \boldsymbol{\Psi} \end{array} \right], \boldsymbol{C} = \left[ \begin{array}{cc} \boldsymbol{\Phi}'' & \boldsymbol{0} \end{array} \right], \boldsymbol{D} = \left[ \begin{array}{c} \boldsymbol{0} \end{array} \right], \boldsymbol{W} = \left[ \begin{array}{c} \boldsymbol{0} \\ \boldsymbol{\Psi} \end{array} \right], \boldsymbol{V} = \left[ \begin{array}{c} \boldsymbol{I} \end{array} \right]. \tag{15}$$

Using a KF [7], the continuous state-space form of the equations is transformed into discrete time form, and optimal estimates are obtained by first predicting the states $\boldsymbol{x}_k^-$ by integrating the discrete system dynamics over a time step, and then correcting the predictions with the output measurements $\hat{\boldsymbol{y}}_k$ as

$$\boldsymbol{x}_k = \boldsymbol{x}_k^- + \boldsymbol{K}_k(\hat{\boldsymbol{y}}_k - \boldsymbol{y}_k^-), \tag{16}$$

$\boldsymbol{K}_k$ being the optimal filter gain matrix [7].

Figure 1 shows the tower tip fore-aft velocity during a simulation in turbulent wind. The solid line is the actual time history computed on the multibody plant model, while the dashed line is the reconstructed value computed using only the first bending tower mode. Realistic values of the noises on accelerometer and strain gage were used in the simulations. Notice that after a filter warm-up of about 10 seconds, the tower tip velocity is captured with good accuracy in its the peak values and phase.

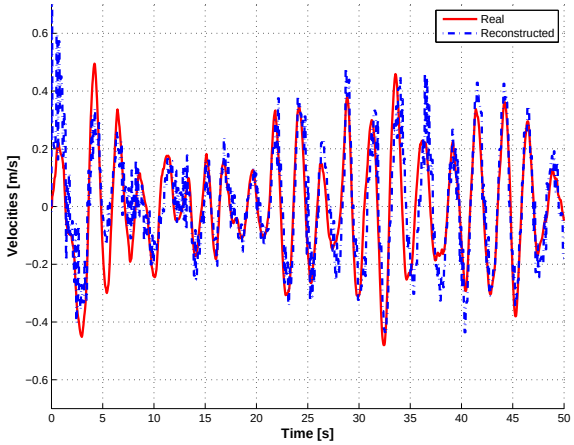


**Figure 1.** KF tower tip velocity estimation. Actual: solid line; reconstructed: dashed line.

## 3. Wind observer

Wind measurements based on the readings of an on board anemometer are typically not reliable enough to be used by pitch and torque controllers. Therefore, wind must be estimated by other means. Estimates of the wind are here used by the model-based controllers, but also by a wind-scheduled PID controller.

In this work the hub wind is reconstructed using an Extended Kalman Filter (EKF) [7]. The wind state equation is simply

$$\dot{V_w} = n_w, \tag{17}$$

where $n_w$ is a white process noise.

The output measurement equation is obtained from the dynamic equilibrium of the rotor, Eq. (1), as

$$y = (J_R + J_G)\dot{\Omega} + T_l(\Omega) + T_{el_e} - T_a(\Omega, \beta_e, V_w - \dot{d}, V_m) + n_v, \tag{18}$$

where $n_v$ is a white measurement noise, and the output $y$ represents the equation residual. All quantities appearing in the previous expression can be measured with good precision. In fact, the rotor speed is provided by a sensor on the shaft; from two successive readings the rotor acceleration is obtained by numerical differentiation. Furthermore, the blade pitch is also accurately measured by a sensor, while the tower fore-aft velocity is reconstructed using the KF procedure described above. Finally, the electrical torque (or the electrical power) is usually available with a good approximation, and the mean wind $V_m$ can be obtained by filtering the reconstructed wind time history with a moving average on a window of 10 seconds.

The non-linear state-space form of the equations is obtained as

$$\begin{cases} \dot{x} &= f(x, \boldsymbol{u}, n_w), \\ y &= h(x, \boldsymbol{u}, n_v), \end{cases} \tag{19}$$

by simply defining $x = V_w$, $\boldsymbol{u} = (\dot{\Omega}, \Omega, \beta_e, \dot{d}, V_m)^T$, and functions $f(\cdot,\cdot,\cdot)$ and $h(\cdot,\cdot,\cdot)$ accordingly, based on Eq. (17) and (18).

According to the EKF algorithm, the continuous state-space form of the equations is transformed into discrete time form, and optimal estimates are obtained by first predicting the states over a time step. Next, the predictions are corrected as in Eq. (16) with the output measurement $\hat{y}_k$ (which is in this case $\hat{y}_k = 0$, since the goal of the wind reconstruction is to drive the residual of the torque balance equation to zero), where the optimal filter gain matrix is now based on the linearization of Eqs. (19) [7].

Figure 2 shows the result of the identification procedure in the case of turbulent wind, while figure 3 reports the case of two successive $\text{EOG}_1$ gusts at 13 m/sec. For both figures, the solid

line is the real wind, while the dashed line represents the observed wind reconstructed with the EKF.

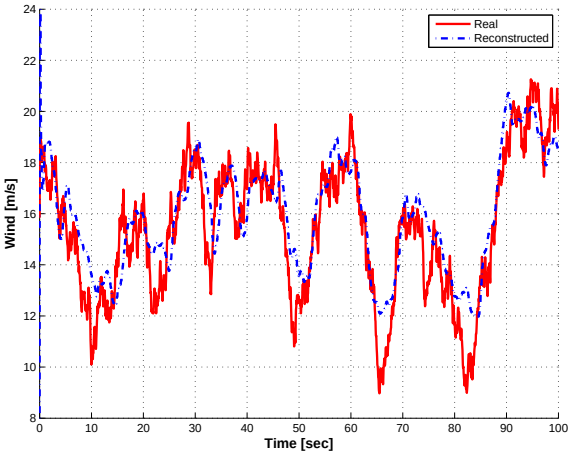


**Figure 2.** EKF turbulent wind estimation. Actual: solid line; reconstructed: dashed line.

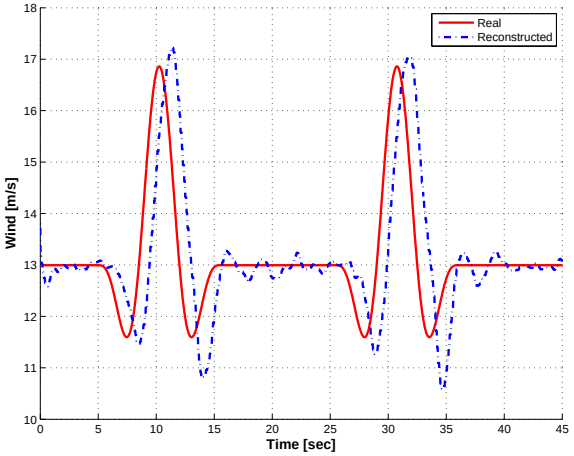


**Figure 3.** EKF gust estimation. Actual: solid line; reconstructed: dashed line.

## 4. Control laws

### *4.1. PID controller*

The proportional-integral-derivative (PID) control strategy is to calculate the collective pitch blade input as

$$\beta_c = K_p(\Omega - \Omega^*) + K_i \int_{t-T_i}^{t} (\Omega - \Omega^*) d\tau + K_d \dot{\Omega}\,, \tag{20}$$

where $K_p$, $K_i$, and $K_d$ are the proportional, integral and derivative gains, respectively, while $\Omega^*$ is the desired rotor speed. The commanded electrical torque input is on the other hand simply tabulated as a function of the rotor angular speed. This control scheme is widely used in practice thanks to its simplicity and robustness. However, the problem of selecting the control gains is not easily solved using simple trial and error strategies, and could lead to sub-optimal performance.

In the present work the PID control gains are optimized using a numerical optimization technique. To this end, a cost function is defined as a weighted sum of equivalent fatigue loads for tower and blades, activation duty cycle, tower fore-aft accelerations, and regulation error on angular speed and generated power. Next, simulations are run in closed-loop with the PID controller in turbulent wind conditions and for given values of the mean wind speed. This cost function is regarded as a sole function of the PID control gains, and it is minimized through a numerical optimization technique using the commercial software Noesis Optimus$^{\text{TM}}$. For efficiency, first a global optimization is performed using the coarse-scale reduced model. Next, the control gains are refined by running a local optimization with the fine-scale aeroelastic model, using a gradient-based method coupled to a response surface approximation of the cost. This yields the optimal gains for the considered mean wind speed. The procedure is repeated for different values of the mean wind, producing a wind-scheduled optimized PID controller.

*4.2. LQR*

The second controller considered in this work is a wind-scheduled MIMO LQR. The reduced model of Eqs. (1–4) can be written in compact form as

$$\dot{\boldsymbol{x}} = \boldsymbol{f}(\boldsymbol{x}, \boldsymbol{u}, V_w, V_m), \tag{21}$$

where the state vector is defined as $\boldsymbol{x} = (d, \dot{d}, \Omega, \beta_e, \dot{\beta}_e, T_{el_e})^T$, while the control inputs are $\boldsymbol{u} = (\beta_c, T_{el_c})^T$.

The controller operates with the same logic on both region 2 and 3, by tracking goal regulation states $\boldsymbol{x}^*(V_m)$ and control inputs $\boldsymbol{u}^*(V_m)$. The goal states and inputs are computed off-line by means of dynamic simulations with the fine-scale aeroelastic model, conducted at varying mean wind speeds $V_m$ and with the turbulent wind component switched off. For each mean wind value, a goal value of the commanded electrical torque $T^*_{el_e}$ is prescribed, chosen in region 2 to maximize the $C_{P_e}$ and in region 3 not to exceed given maximum loads. Set a goal value of rotor speed $\Omega^*$, a simulation is run until all transients have decayed and a periodic solution is reached under the action of the PID controller of the previous section. The steady regulation values of the remaining control and states are then obtained by averaging over a rotor revolution the periodic time histories.

At each one of these regulation states, a linearized reduced model is computed from the non-linear one expressed by Eq. (21). This defines a wind-parameterized linear model

$$\Delta\dot{\boldsymbol{x}} = \boldsymbol{A}(V_w, V_m)\Delta\boldsymbol{x} + \boldsymbol{B}(V_w, V_m)\Delta\boldsymbol{u}, \tag{22}$$

$\Delta\boldsymbol{x} = \boldsymbol{x} - \boldsymbol{x}^*(V_m)$, $\Delta\boldsymbol{u} = \boldsymbol{u} - \boldsymbol{u}^*(V_m)$, from which, given a quadratic cost function

$$J = \frac{1}{2}\int_0^\infty \left(\Delta\boldsymbol{x}^T\boldsymbol{Q}\Delta\boldsymbol{x} + \Delta\boldsymbol{u}^T\boldsymbol{R}\Delta\boldsymbol{u}\right)\,\mathrm{d}t, \tag{23}$$

we compute a wind-scheduled LQR feedback gain matrix $\boldsymbol{K}(V_w, V_m)$ [4], which is stored in table look-up form.

The closed-loop controller is then implemented on-line as $\boldsymbol{u} = -\boldsymbol{K}(V_w, V_m)(\boldsymbol{x} - \boldsymbol{x}^*(V_m))$, where the tower states in the state vector $\boldsymbol{x}$ are reconstructed using the KF filter described above, $V_w$ is the turbulent wind estimate provided by the EKF wind observer and $V_m$ its filtered mean, while the gain matrix is interpolated within the stored table look-up entries.

*4.3. RAPC*

The Reference Augmented Predictive Controller (RAPC) is a receding horizon non-linear adaptive model-based controller which is described in detail in Ref. [3]. RAPC uses two adaptive neural elements, one for improving a reference reduced model and the other for improving a reference control law. Space limitations prevent a detailed treatment of the formulation, and here we only briefly describe the control adaption problem, while the reader is referred to [3] for all details about the model adaption procedure.

Given a cost function defined on the prediction horizon $[t_0, t_0 + T_p]$

$$J = \frac{1}{2}\int_{t_0}^{t_0+T_p} L(\boldsymbol{x} - \boldsymbol{x}^*, \boldsymbol{u} - \boldsymbol{u}^*)\,\mathrm{d}t, \tag{24}$$

the optimal control function is assumed to be in the form

$$\boldsymbol{u} = \boldsymbol{u}_{\mathrm{ref}} + \boldsymbol{\upsilon}_p(\boldsymbol{x}_0, \boldsymbol{x}^*, \boldsymbol{u}^*, t, \boldsymbol{p}_C), \tag{25}$$

where $\boldsymbol{u}_{\mathrm{ref}}$ is a reference given control law (the LQR of the previous section, in this case), and $\boldsymbol{\upsilon}_p$ a parametric function whose free parameters $\boldsymbol{p}_C$ are identified on-line in order to minimize $J$.

Using standard variational arguments, the governing optimal control differential equations are readily found:

$$\dot{\boldsymbol{x}} = \boldsymbol{f}(\boldsymbol{x}, \boldsymbol{u}, V_w, V_m, \boldsymbol{p}_M) = 0, \quad t \in [t_0, t_0 + T_p], \tag{26}$$

$$\boldsymbol{x}(t_0) = \boldsymbol{x}_0, \tag{27}$$

$$-\dot{\boldsymbol{\lambda}} + (\boldsymbol{f}_{,\boldsymbol{x}} + \boldsymbol{u}_{\mathrm{ref},\boldsymbol{x}}^T \boldsymbol{f}_{,\boldsymbol{u}})^T \boldsymbol{\lambda} + L_{,\boldsymbol{x}} + \boldsymbol{u}_{\mathrm{ref},\boldsymbol{x}}^T L_{,\boldsymbol{u}} = 0, \quad t \in [t_0, t_0 + T_p], \tag{28}$$

$$\boldsymbol{\lambda}(t_0 + T_p) = 0, \tag{29}$$

$$\hat{J}_{,\boldsymbol{p}_C} = \int_{t_0}^{t_0+T_p} \boldsymbol{v}_{,\boldsymbol{p}_C}^T (L_{,\boldsymbol{u}} + \boldsymbol{f}_{,\boldsymbol{u}}^T \boldsymbol{\lambda}) \, \mathrm{d}t = 0. \tag{30}$$

The reduced model is expressed by Eq. (26), which is obtained by Eqs. (1–4) with the addition of a parametric function with free model parameters $\boldsymbol{p}_M$ [3] used for the adaption of the reduced model. The unknown parameters $\boldsymbol{p}_C$ are identified through the following iterative process:

(i) *State prediction.* Integrate the current estimate of the reduced model equations (26) forward in time over the prediction window starting at the actual initial condition (27).

(ii) *Co-state prediction.* Using the augmented control function and the states computed at the previous step, integrate the adjoint equations (28) backward in time starting from the final conditions (29).

(iii) *Control parameter update.* Correct current estimate of the control parameters to seek the enforcement of the transversality condition, by using the steepest descent rule:

$$\boldsymbol{p}_C = \boldsymbol{p}_C - \eta_C \, \hat{J}_{,\boldsymbol{p}_C}, \tag{31}$$

where $\eta_C > 0$ is the step length.

(iv) *Plant steering.* Feed the computed controls to the plant, steering it on the window $[t_0, t_0 + T_s]$.

(v) *Model parameter update.* Every $N$ steps, $N \geq 1$, update the model parameter estimate $\boldsymbol{p}_M$.

(vi) Update initial time as $t_0 = t_0 + T_s$, update initial conditions, and repeat from (i).

Here again tower states and wind are provided by the described observers, while the goal states and inputs are computed as for the LQR case.

RAPC is a non-linear predictive controller, yet the number of operations per activation of the controller is fixed, so that it can be implemented in a hard-real-time environment. Furthermore, RAPC is adaptive, yet the neural elements are only trained to capture the defects of given reference elements; if these are well chosen, the defects are small and hence the adaption is fast and can be performed on-line, without necessity of any pre-training [3].

## 5. Results

Extensive tests were run with the multibody model operating in closed-loop with the different controllers in various operating conditions. Space limitations preclude a detailed analysis, and only the main conclusions are reported here.

Figure 4 shows the normalized value of total regulation error accumulated throughout 600 sec simulations in turbulent wind of varying mean intensity. The plot covers both region 2 and 3 conditions, the rated speed being 10.6 m/sec. The plant model is simulated with cold air and ice accretion on the blades, which is modeled as a degraded performance of the airfoil properties; such off-design conditions are unknown to both the PID controller and the model-based ones, which use nominal values of the parameters. In such severe cases, it appears that the predictive controllers outperform the PID one, and RAPC, with its non-linear effects and

adaptive capabilities, further improves on the LQR performance. On the other hand, these difference are significantly less pronounced when operating in nominal conditions, i.e. close to the operating points were the PID gains were optimized and where the reduced models are quite faithful to the plant.

Figure 5 plots the time histories of the plant response in terms of rotor speed for two consecutive $EOG_1$ gusts at 13 m/sec, in nominal conditions. Even in this case, RAPC is significantly better than LQR, which is in turn significantly better than PID.

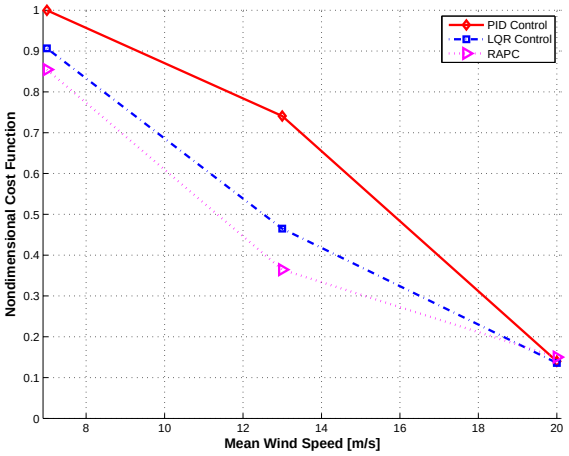


**Figure 4.** Performance comparison in turbulent wind with cold air and ice accretion.

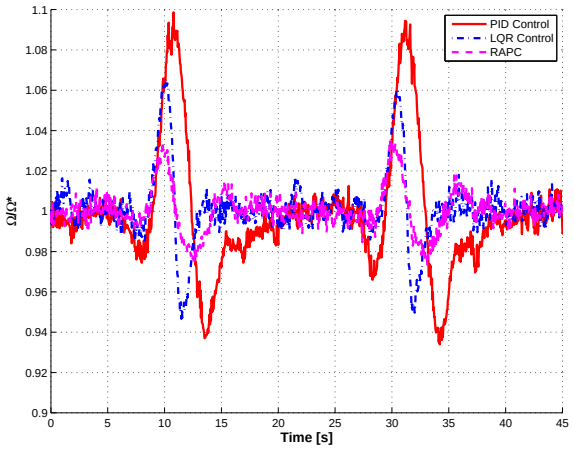


**Figure 5.** Performance comparison in gusty wind in nominal conditions.

Overall, it appears that it is difficult to significantly improve a well tuned simple PID controller when operating in turbulent wind in nominal conditions. On the other hand, there seems to be a significant advantage in using model-based controllers, and specifically non-linear and adaptive ones, when operating in off-design conditions or in the presence of gusts with large wind variations.

## Acknowledgements

This research is supported by Leitner S.p.A, Matteo Casazza project monitor, through a contract with the Politecnico di Milano. This support is gratefully acknowledged.

## References

[1] 1999 Wind turbine generator system — Part I: Safety requirements *International Standard IEC 61400-1.*
[2] Bauchau OA, Bottasso CL and Nikishkov YG 2001 Modeling rotorcraft dynamics with finite element multibody procedures *Math. Comput. Model.* **33** 1113-37.
[3] Bottasso CL, Nicastro R, Savini B, Riviello L 2007 Adaptive reference-augmented predictive control, with application to the reflexive control of unmanned rotorcraft vehicles *IEEE Transactions on Automatic Control* under review.
[4] Mosca E 1995 *Optimal, Predictive and Adaptive Control* (Englewood Cliffs: Prentice Hall)
[5] Peters DA and He CJ 1995 Finite state induced flow models – Part II: Three-dimensional rotor disk *J. Airc.* **32** 323-33.
[6] Powles SRJ 1983 The effects of tower shadow on the dynamics of a horizontal-axis wind turbine *Wind Eng.* **7** 26-42.
[7] Zarchan P and Musoff H 2005 *Foundamentals of Kalman Filtering: a Practical Approach* Progress in Astronautics and Aeronautics Series **208** (AIAA).